Progress In Electromagnetics Research C, Vol. 28, 209–222, 2012

SYSTEMATIC CALIBRATION OF TWO-PORT NETWORK ANALYZER FOR MEASUREMENT AND ENGINEERING OF WAVEFORMS AT RADIO FREQUENCY

W. S. El-Deeb[1, 2], M. S. Hashmi[2, 3, *], N. Boulejfen[2, 4], and F. M. Ghannouchi[2]

[1]Zagazig University, P. O. Box 4451, Zagazig, Egypt

[2]iRadio Lab, University of Calgary, Calgary, T2N 1N4, Canada

[3]IIIT Delhi, Sector-3, Dwarka, New Delhi 110078, India

[4]King Faisal University, P. O. Box 380, Ahsaa 31982, KSA

Abstract—This paper reports algorithm and technique for the accurate phase calibration in order to measure current and voltage waveforms at the terminals of two-port microwave devices. The calibration approach presented in this paper does not require any multi-harmonic coherent signal generator and golden standard, reported in earlier papers, thus allowing the system to be more reliable, generic and accurate. The results achieved using the reported calibration algorithm on a developed measurement setup shows good agreement with those obtained on a standard commercial scope. In the end, it has been shown that the developed algorithm and measurement setup can be adapted for carrying out waveform engineering which clearly identifies the application of this work in the characterization and measurement of microwave devices.

1. INTRODUCTION

Time-domain waveform measurements and engineering technique has established its importance in the characterization of microwave power devices and design of power amplifiers [1–4]. They provide good understanding of device behavior and also generate extremely useful data for the investigation of device behavior and its nonlinear modeling using modern computer aided design tools [5, 6]. The ability to

Received 8 March 2012, Accepted 9 April 2012, Scheduled 13 April 2012

* Corresponding author: Mohammad S. Hashmi (mshashmi@ucalgary.ca).

visualize waveforms helps in the determination of the optimal device operating point and performance, whereas the shape of the waveform aids the amplifier designers in determining the appropriate input and output impedances and, in turn, the matching circuits. The waveform measurement systems are also useful in the determination of operating classes of power amplifiers such as class-F and class-F^{-1} [7, 8].

The waveform measurement systems rely on the ease, accuracy and flexibility of the associated calibration algorithms for the overall confidence in the measured data. In principle the calibration algorithm used for error correction in a vector network analyzer (VNA) [9] is only appropriate for measurements on the ports of linear device under test (DUT). In the VNA calibration, all the individual error terms are not required considering that measurements are carried out to measure the ratio of traveling waves at the DUT ports. However, the measurement of current and voltage waveforms at the ports of nonlinear DUTs require absolute knowledge of phase and amplitudes of each error terms at each harmonic component in order to accurately extract the waveforms from the measured traveling waves.

There have been several techniques such as power de-embedding [10] that can determine the absolute magnitudes of individual error terms. However, most of the time the determination of absolute phase values of the error terms at harmonic frequencies rely on a certain type of nonlinear golden standard in achieving the desired accuracy in phase calibration and measurements. Some of the systems rely on step recovery diode (SRD) [1] while some others rely on active device based standard phase reference generators [11–14]. There has been report of alternative calibration technique [15] that requires several procedural steps in order to perform the necessary calibration, but this is a tedious process and is not straightforward. Majority of the reported algorithm are not generic, are cumbersome and time consuming.

The calibration algorithm reported in this paper eliminates the need for the phase reference generator in the calibration process and thus achieves inherent accuracy and reliability. The developed algorithm is simpler and requires less computation steps and thus significantly expedites the measurement and calibration time. Furthermore, the calibration algorithm does not rely on the use of harmonic generator to achieve accurate waveform measurements. Additionally, this paper reports the use of the calibration algorithm on a multi-harmonic phase-locked receiver (MHR) in the development of a reliable waveform measurement system. Overall, this paper provides an enhanced waveform measurement system for the characterization, measurement, and modeling of microwave devices.

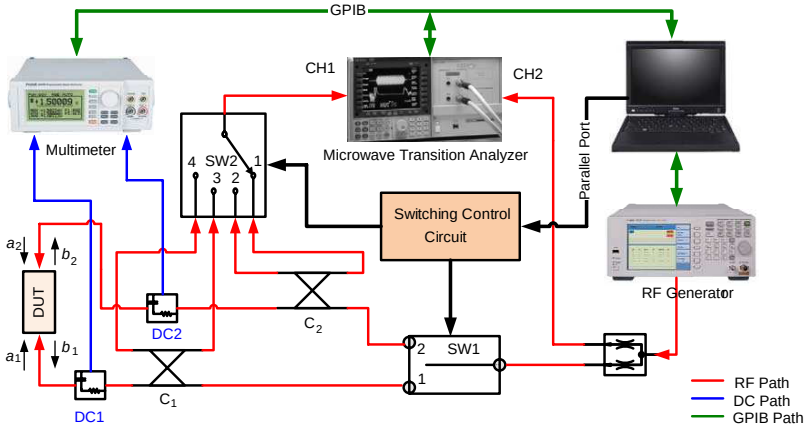

Figure 1. Block diagram of the proposed measurement system.

2. DESCRIPTION OF THE MEASUREMENT SETUP

The proposed waveform measurement system is shown in Figure 1. To validate the ability of the proposed calibration algorithm to provide accurate waveform measurements, a setup has been built around a two channel MHR. A harmonic receiver operates in a similar way to a conventional superheterodyne receiver; the main difference is in the mixing process. In a harmonic receiver the local oscillator signal is first passed though a comb generator prior to being applied to the mixer. This effectively generates multiple harmonics of the local oscillator signal meaning that multiple sections of RF spectrum can be simultaneously captured. Microwave Transition Analyzer (MTA) works as MHR in this measurement setup but the developed calibration algorithm described in this paper is equally applicable for any other MHR.

The radio frequency (RF) signal is routed to the device under test (DUT) from the RF source via switch 1 (SW1). The sampled incident and reflected waves are sent to the first channel of the MHR, CH1, via switch 2 (SW2). The second channel of the MHR, CH2, is used as a reference channel by receiving a sample from the RF signal coming from the source via the power divider. The switching matrix is controlled using the parallel port of the personal computer (PC) via a programmable peripheral interface (PPI, Intel 82C55A). The RF generator and MHR are controlled with a general purpose interface bus. In the setup, the measurements are performed at the MHR as ratios between CH1, as the receiver of the incident and reflected waves to be measured, and CH2, as a reference channel.

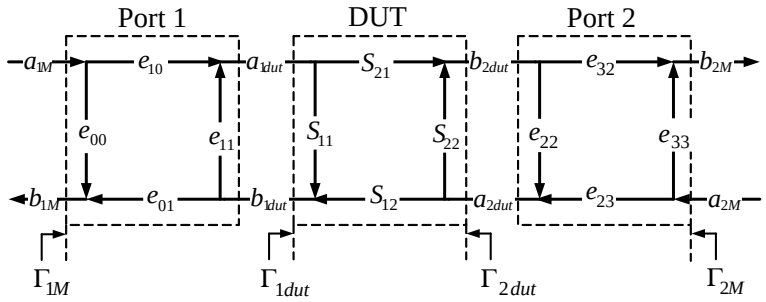

Figure 2. Error flow graph depicting the error terms between the DUT and MHR ports.

3. SYSTEM CALIBRATION

The error signal flow graph depicting the error boxes between the DUT and the MHR is shown in Figure 2. The terms with subscript M refers to the measured quantities at the port of MHR, whereas the terms with subscript dut refer to the quantities at the DUT ports. The voltage and current waveforms at the ports of DUT are related to the traveling waves at the respective ports. For example, the respective voltage and current at port 1 of the DUT is given by Equations (1) and (2).

$$V_{1dut} = \sqrt{Z_0}(a_{1dut} + b_{1dut}) \tag{1}$$

$$I_{1dut} = \frac{(a_{1dut} - b_{1dut})}{\sqrt{Z_0}} \tag{2}$$

Accurate extraction of waveforms requires the determination of traveling waves at the DUT ports in terms of the measured traveling waves at the MHR ports. Error flow graph given in Figure 2 can be solved to determine the relationships, given in Equations (3) and (4), between the traveling waves at the MHR ports and the port 1 of the DUT.

The error parameter $e_{10}e_{01}$, in Equations (3) and (4), represents the reflection tracking for the error box between port 1 of the MHR and port 1 of the DUT. It consists of two factors; e_{10} which represents the forward-loss from the measuring instrument and the DUT port, while e_{01} represents the reveres-loss from port 1 of the DUT to the port 1 of the MHR. Both values of e_{10} and e_{01} are complex and they affect the magnitude and the phase of the RF signal hitting port 1 of

the DUT.

$$a_{1dut} = \left(\frac{e_{01}e_{10} - e_{00}e_{11}}{e_{01}}\right) a_{1M} + \left(\frac{e_{11}}{e_{01}}\right) b_{1M} \tag{3}$$

$$b_{1dut} = \left(\frac{-e_{00}}{e_{01}}\right) a_{1M} + \left(\frac{1}{e_{01}}\right) b_{1M} \tag{4}$$

The denominator in Equations (3) and (4) contains only the value of e_{01}, which means that; it is necessary to calculate the error parameter e_{01} separately in order to get the correct phase of the incident and reflected waves at the DUT. This is because the phase of e_{01} can not be extracted from the phase of the error parameter $(e_{10}e_{01})$ calculated as one-term without calculating the second error parameter e_{10}. It is evident from Equations (3) and (4) that the determination of incident and reflected traveling waves at the DUT port 1 requires knowledge of individual terms of the error flow graph, especially for the error term e_{01} in Equations (3) and (4) as described. Therefore an enhanced calibration, which determines the absolute phase and magnitude values of each error terms, needs to be carried out in the measurement system in order to accurately extract the waveforms at the ports of the DUT.

This section describes the two step calibration process for calculation of the error terms. Similar expressions that relate error terms of error box between the MHR and port 2 of the DUT and traveling waves at port 2 of the DUT can also be derived [2].

3.1. First Calibration Step (*S*-Parameter Calibration)

The first step is the usual VNA type calibration for the determination of error terms e_{00}, e_{11} and $e_{01}e_{10}$. For the first port measurement, following expression relating the reflection coefficient at the MHR port, Γ_M, and reflection coefficient at the first port of DUT, Γ_{dut}, can be derived from Figure 2.

$$\Gamma_{1M} = e_{00} + \frac{e_{01}e_{10}\Gamma_{1dut}}{1 - e_{11}\Gamma_{1dut}} = \frac{-\Delta e\Gamma_{1dut} + e_{00}}{-e_{11}\Gamma_{1dut} + 1} \tag{5}$$

$$\text{where, } \Delta e_1 = (e_{00}e_{11} - e_{01}e_{10}) \,. \tag{6}$$

Measurement of open-short-load (OSL) standards at port 1 and application of (5) gives three set of linear equations which are summarized as Equation (7) in matrix form.

$$\begin{bmatrix} e_{00} \\ e_{11} \\ \Delta e_1 \end{bmatrix} = \begin{bmatrix} 1 & \Gamma_O \times \Gamma_{MO} & -\Gamma_O \\ 1 & \Gamma_S \times \Gamma_{MS} & -\Gamma_S \\ 1 & \Gamma_L \times \Gamma_{ML} & -\Gamma_L \end{bmatrix}^{-1} \times \begin{bmatrix} \Gamma_{MO} \\ \Gamma_{MS} \\ \Gamma_{ML} \end{bmatrix} \tag{7}$$

where:
Γ_{MO}: the measured value of the open standard.

Γ_{MS}: the measured value of the short standard.
Γ_{ML}: the measured value of the load standard.
Γ_O: the value of the open standard, which equals 1.
Γ_S: the value of the short standard, which equals -1.
Γ_L: the value of the load standard, which equals 0.

The error terms e_{00}, e_{11} and $e_{01}e_{10}$ between the port 1 of the DUT and the MHR can then be calculated using Equation (7). The error terms e_{33}, e_{22} and $e_{23}e_{32}$ between the port 2 and MHR can be obtained by connecting a THRU standard between port 1 and port 2 as shown in Figure 2. The error terms e_{33}, e_{22} and $e_{23}e_{32}$ as a function of the measured S-parameters of the THRU standard is given in Equations (8)–(11).

$$e_{33} = \frac{S_{11T} - e_{00}}{t_{11} + e_{11}(S_{11T} - e_{00})} \tag{8}$$

$$e_{22} = S_{22T} - \frac{t_{22}e_{11}}{1 - e_{11}e_{33}} \tag{9}$$

$$t_{11} = e_{01}e_{10} = e_{00}e_{11} - \Delta e_1 \tag{10}$$

$$t_{22} = e_{32}e_{23} = S_{12T}S_{21T}\frac{(1 - e_{11}e_{33})^2}{t_{11}} \tag{11}$$

where S_{11T}, S_{12T}, S_{21T}, and S_{22T} are the measured S-parameters of the THRU standard connected between port 1 and port 2, and t_{11} and t_{22} are the reflection tracking parameters representing ports 1 and 2, respectively.

Equations (7) and (8)–(11) allows the calculation of error terms e_{00}, e_{11}, e_{22}, e_{33}, $e_{01}e_{10}$ and $e_{23}e_{32}$ of the error boxes between the MHR and the DUT ports, and is therefore referred as the S-parameter calibration stage. These calculations of the error box parameters enable the extraction of the incident and reflected traveling waves at the DUT ports using power de-embedding [9]. The power de-embedding allows the possibility of relating the phase of fundamental component to the phase values of distinct harmonic components and therefore this measurement technique is called relative waveform extraction technique [2].

However the measured waveforms using power de-embedding technique may not represent the actual waveform present at the DUT ports due to phase ambiguity considering that the this approach although allows the determination of magnitudes of individual error terms but the phase of error terms e_{01} and e_{10} or e_{32} and e_{23} are still calculated as one error parameter $e_{01}e_{10}$ or $e_{23}e_{32}$, respectively. In practice, the phase ambiguity does not have a big effect, especially when the power amplifier works in its linear region; but this can show significant ambiguity in the waveforms when the power amplifier (PA)

works in the nonlinear region, as demonstrated in the measurement validations section. Therefore to address this concern, absolute phase and magnitude of each error terms are required which we term as enhanced calibration procedure described in next section.

3.2. Second Calibration Step (Enhanced Calibration)

With the THRU standard connected between ports 1 and 2 in the second step, the two possible values of $e_{01}e_{10}$ can be calculated using (12) and (13) as follows [15, 16].

$$S_{21T}(e_{10}e_{23})^2 - S_{12T}(e_{01}e_{10})(e_{23}e_{32}) = 0 \tag{12}$$

$$e_{10}e_{23} = \pm\sqrt{\frac{S_{12T}(e_{01}e_{10})(e_{32}e_{23})}{S_{21T}}}\,. \tag{13}$$

Knowing the length of the THRU standard, the appropriate solution for the transmission tracking between the first and second DUT ports, $e_{01}e_{23}$, can be selected using the inequality represented in (14)

$$Re\left[\frac{e^{-\gamma l}}{S_{21T}}\right] > 0 \tag{14}$$

where γ is the propagation constant, l is the length of the THRU standard and S_{21} is the measured S-parameter of the THRU standard connected between ports 1 and port 2.

In this calibration step, a coaxial cable with known S-parameters is connected between port 1 of the DUT and the measuring port of the MHR. This calibration step is key point in the determination of the absolute values of e_{01} and e_{10}. Connecting the coaxial cable between port 1 of the DUT and the measuring port of the MHR gives the ability to measure directly the traveling wave, b_{coax}, at port 1 of the DUT. Figure 3 indicates that the measured traveling wave, b_{coax}, is function of the error parameters of the first error box and the S-parameters of

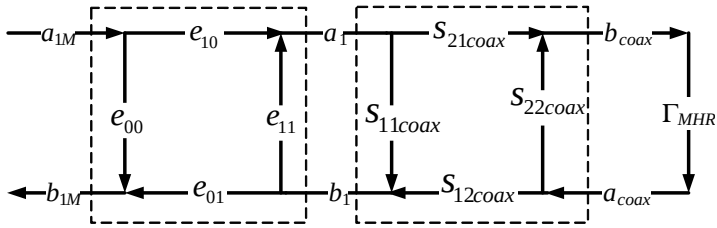

Figure 3. Error flow graph of the setup with coaxial cable between the MHR and port 1 of the DUT.

the coaxial cable as given in Equation (15). The S-parameters of the coaxial cable can be either measured by a calibrated VNA or by the setup developed up to second calibration step described in this paper.

The error flow graph in Figure 3 can be solved using Mason's rule to obtain the expression for the error term e_{10} given in Equation (15).

$$e_{10} = \left(\frac{b_{coax}}{a_{1M}}\right)\left(\frac{(1-e_{11}S_{11Coax})(1-\Gamma_{MHR}S_{22coax})}{S_{21coax}}\right) - \left(\frac{b_{coax}}{a_{1M}}\right)\left(\frac{(e_{11}\Gamma_{MHR}S_{21coax}S_{12coax})}{S_{21coax}}\right) \quad (15)$$

The determination of absolute value of individual term e_{01} enables the calculation of error parameters from Equations (16)–(18) which are obtained from simplifications of Equations (10), (11), (13) and (15).

$$e_{01} = \frac{e_{01}e_{10}}{e_{10}} = \frac{t_{11}}{e_{10}} \quad (16)$$

$$e_{23} = \frac{e_{10}e_{23}}{e_{10}} \quad (17)$$

$$e_{32} = \frac{e_{23}e_{32}}{e_{23}} = \frac{t_{22}}{e_{23}} \quad (18)$$

Once the error parameters have been calculated, the incident and reflected waves at ports 1 and 2 of the DUT, shown in Figure 2, can be de-embedded using (3), (4), (19) and (20), respectively.

$$a_{2dut} = \left(\frac{e_{32}e_{23}-e_{33}e_{22}}{e_{23}}\right)a_{2M} + \left(\frac{e_{33}}{e_{23}}\right)b_{2M} \quad (19)$$

$$b_{2dut} = \left(\frac{-e_{33}}{e_{23}}\right)a_{2M} + \left(\frac{1}{e_{23}}\right)b_{2M} \quad (20)$$

The extraction of incident and reflected waves at each port of the DUT allows the accurate measurements of current and voltage waveforms, from Equations (1) and (2), at port 1 and port 2 of the DUT.

4. MEASUREMENT VALIDATIONS

4.1. Waveform Measurements

The calibration algorithm and the measurement system have been verified using a medium high power Mini-Circuits ZHL-42W power amplifier, which was driven at 0.5 GHz with a 17 V DC bias while considering up to five harmonics. To demonstrate the functionality of the developed waveform measurement system, the amplifier was driven at different input power levels, so that the measurement

could be carried out and verified in the linear and nonlinear regions of the power amplifier operation. The obtained waveforms have been compared to those obtained from a commercial 4 Gbps digital oscilloscope (Tektronix TDS 794D) [18], for validation of the voltage time-domain waveforms at the DUT ports.

The measured voltage waveforms using the commercial scope and the developed system based on enhanced calibration algorithm show a good agreement when the amplifier is operated under linear mode, Figure 4, while there is slight difference in the nonlinear operation, Figure 5, considering that the developed system captured all the spectral component of the voltage waveform whereas the scope could capture spectral lines only up to the four harmonics for the chosen excitation of 500 MHz due to limited bandwidth of the commercial scope.

To visualize the accuracy achieved in the measured voltage waveform using the enhanced calibration reported in this paper, the

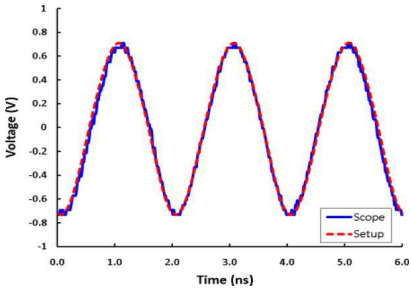

Figure 4. Output voltage waveforms of the ZHL-42 power amplifier at −9 dBm input power.

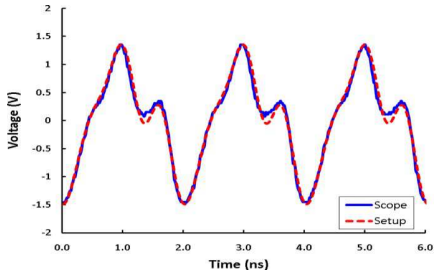

Figure 5. Output voltage waveforms of the ZHL-42W power amplifier at −3 dBm input power.

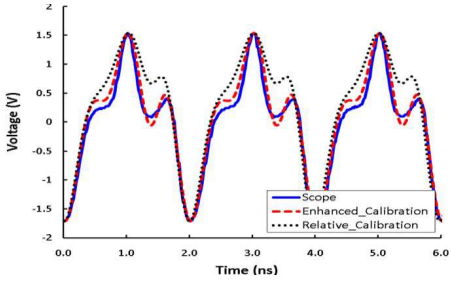

Figure 6. Output voltage waveforms of the ZHL-42W power amplifier at 0 dBm input power.

obtained voltage waveforms in the nonlinear operation mode of ZHL-42W when compared to those obtained under similar bias and drive conditions using the commercial scope and the relative calibration algorithm [2]. It is evident from Figure 6 that the voltage waveform obtained using the relative calibration algorithm is way off the target when compared to those obtained using commercial scope. The enhanced calibration and the commercial scope show better agreements with the difference only emanating due to the limited bandwidth of the commercial scope.

4.2. Waveform Engineering

To evaluate the waveform engineering capability of the developed measurement system, a gallium nitride (GaN) 28 V, 4 W high electron mobility transistor (HEMT, NPTB00004) [20] mounted on a fixture (Focus Microwaves PTJ-X-N) was measured in a non-50 Ω impedance environment. The non-50Ω impedance can be created by load-pull system [21–23], but in this case a simple coaxial harmonic tuner (Maury Microwave Corporation 2612C2) was connected at the output port of the transistor to generate the required non-50 Ω impedances. The transistor was biased at $V_{gs} = -1.4$ V and $V_{ds} = -28$ V through the bias tees connected to the drain and gate of the transistor.

The output current and voltage waveforms, measured at three different output impedances, are shown in Figure 9. The output impedances for these cases have been measured for a fundamental frequency of 1 GHz and four harmonics at an input power of 20 dBm, as indicated in Table 1. It is evident from Figure 7 that the system is able to measure the voltage and current waveforms for different load impedances. The transistor gives a quasi distortion-free voltage and current waveforms at its optimum load impedance, case 1 in Table 1

Table 1. Output reflection coefficient measurements of the power amplifier at 1 GHz fundamental frequency and 4 harmonics.

Case	Output Reflection Coefficient				
	$@f_o$	$@2f_o$	$@3f_o$	$@4f_o$	$@5f_o$
Case 1	0.63 $\angle 41.9°$	0.788 $\angle 110.8°$	0.347 $\angle -61.1°$	0.234 $\angle 92.4°$	0.736 $\angle -0.4°$
Case 2	0.26 $\angle -15.5°$	0.78 $\angle 110.3°$	0.58 $\angle -128.5°$	0.196 $\angle 78.8°$	0.75 $\angle -1.5°$
Case 3	0.786 $\angle -70.4°$	0.805 $\angle -3.4°$	0.33 $\angle 11.52°$	0.207 $\angle 98.9°$	0.21 $\angle 12.8°$

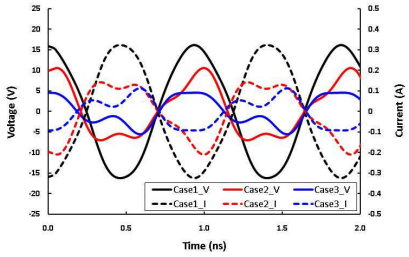

Figure 7. Measured waveforms for different output impedances at 20 dBm input power for an NPTB00004 GaN HEMT transistor at a fundamental frequency of 1 GHz.

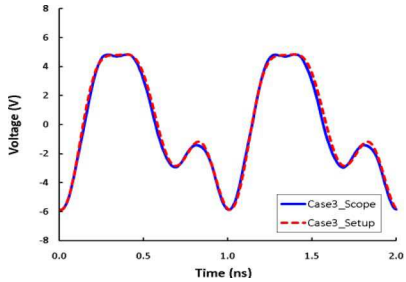

Figure 8. Comparison between the measurements of the scope and the developed system for the waveform of case 3.

and Figure 7, generated by the harmonic tuner at the transistor output. The distortions in waveforms start to appear when the impedances are varied to non-optimal values, cases 2 and 3. As a consequence, the transistor begins to lose its gain and behaves in nonlinear manner.

In order to validate the measured output waveform in a non 50 Ω environment and to increase the trust in the measurement, the measured waveform of case 3 was compared with the measured voltage waveform using a commercial 18 Gbps high-speed scope, (Hewlett Packard 54750A) [24] under similar operating conditions. The results in Figure 8 show good agreement; thus, it can be concluded that the developed waveform measurement and engineering system can be trusted during its deployment in microwave device optimization, characterization and measurements.

5. CONCLUSION

This paper presented a comprehensive calibration procedure for waveform measurements, based around a two-channel receiver setup. The developed calibration strategy discards the use of the golden standard and, thus, significantly improves the existing calibration techniques reported earlier [7, 9, 13]. It has been systematically proven that the developed calibration procedure and measurements provide accurate results. The measurements carried out by this setup can therefore be trusted when deployed in the application of microwave characterization. The significance of the determination of the phase of the error parameters, e_{01} and e_{10}, has been demonstrated through

measurement results.

The proposed calibration algorithm utilizes a standard signal frequency generator and does not rely on the use of a multi harmonic generator to calculate the error box parameters at fundamental and harmonic frequencies. The algorithm is also applicable to any multi harmonic phase-locked receiver based measurement system.

Finally, it has been demonstrated that the measurement system is capable of performing waveform engineering measurements. The comparison of waveforms obtained in $50\,\Omega$ and non $50\,\Omega$ impedance environments, using the developed system and the standard commercial scopes, shows good agreement. This enhances confidence in the measurement data obtained from the developed measurement system.

REFERENCES

1. Bensmida, S., P. Poire, R. Negra, F. M. Ghannouchi, and G. Brassard, "New time-domain voltage and current waveform measurement setup for power amplifier characterization and optimization," *IEEE Transaction on Microwave Theory and Techniques*, Vol. 56, No. 1, 224–231, January 2008.
2. El-Deeb, W. S., M. S. Hashmi, S. Bensmida, N. Boulejfen, and F. M. Ghannouchi, "Thru-less calibration algorithm and measurement system for on-wafer large-signal characterization of microwave devices," *IET Microwaves, Antenna and Propagation*, Vol. 4, No. 11, 1773–1781, November 2010.
3. Hashmi, M. S., A. L. Clarke, S. P. Woodington, J. Lees, J. Benedikt, and P. J. Tasker, "An accurate calibrate-able multi-harmonic active load-pull system based on the envelope load-pull concept," *IEEE Transaction on Microwave Theory and Techniques*, Vol. 58, No. 3, 656–664, March 2010.
4. Hashmi, M. S., A. L. Clarke, P. J. Helaoui, P. J. Tasker, and F. M. Ghannouchi, "Agile harmonic envelope load-pull system enabling reliable and rapid device characterization," *Measurement Science and Technology*, Vol. 21, No. 5, 1–9, 2010.
5. Ramadan, A., T. Reveyrand, A. Martin, J. M. Nebus, P. Bouysse, L. Lapierre, J. F. Villemazet, and S. Forestier, "Experimental study on effect of second-harmonic injection at input of classes of F and F-1 GaN power amplifiers," *IET Electronic Letter*, Vol. 46, No. 8, 570–572, April 15, 2010,
6. Ghannouchi, F. M. and M. S. Hashmi, "Experimental investigation of the uncontrolled higher harmonic impedances effects on the

performance of high power microwave devices," *Microwave and Optical Technology Letters*, Vol. 52, No. 11, 2480–2482, November 2010.

7. Raab, F. H., "Class-F power amplifiers with maximally flat waveforms," *IEEE Transaction on Microwave Theory and Techniques*, Vol. 45, No. 11, 2007–2012, November 1997.
8. Rhodes, J. D., "Output universality in maximum efficiency in linear power amplifier," *International Journal on Circuit Theory and Applications*, Vol. 31, 385–405, 2003.
9. Agilent Application Note, "Applying error correction to network analyzer measurements," 1998, http://cp.literature.agilent.com/litweb/pdf/5965-7709E.pdf.
10. Bousnina, S., C. Falt, P. Mandeville, A. B. Kouki, and F. M. Ghannouchi, "An accurate on-wafer deembedding technique with application to HBT devices characterization," *IEEE Transactions on Microwave Theory and Techniques*, Vol. 50, No. 2, 420–424, February 2002.
11. Wei, C. J., Y. A. Tkachenko, and D. Bartle, "Waveform measurement technique and its applications to optimum loading studies on power FETS," *International Conference on Microwave and Millimeter Wave Technology*, 666–669, 2002.
12. Kompa, G. and F. van Raay, "Error-corrected large-signal waveform measurement system combining network analyzer and sampling oscilloscope capabilities," *IEEE Transaction on Microwave Theory and Techniques*, Vol. 38, No. 4, 358–365, April 1990.
13. Lott, U., "Measurement of magnitude and phase of harmonics generated in nonlinear microwave two-ports," *IEEE Transaction on Microwave Theory and Techniques*, Vol. 37, No. 10, 1506–1511, October 1989.
14. Sipila, M., K. Lehtinen, and V. Porra, "High-frequency periodic time-domain waveform measurement system," *IEEE Transaction on Microwave Theory and Techniques*, Vol. 36, No. 10, 1397–1405, October 1988.
15. Williams, D. J. and P. J. Tasker, "An automated active source and load-pull measurement system," *Proc. 6th IEEE High Frequency Student Colloquium*, 7–12, Cardiff, UK, September 2001.
16. Blockley, P. S. and J. G. Rathmell, "Towards generic calibration," *65th Spring ARFTG Conference Digest*, 1–5, June 2005.
17. Wei, C. J., Y. A. Tkachenko, and D. Bartle, "Waveform measurement technique and its applications to optimum loading

studies on power FETS," *International Conference on Microwave and Millimeter Wave Technology*, 666–669, 2002.

18. Tektronix TDS794D User's Manual, http://www2.tek.com/cms wpt/psdetails.lotr?ct=PS&cs=psu& ci=13446&lc=EN.
19. Stancliff, R. B. and D. P. Poulin, "Harmonic load-pull," *IEEE MTT-S International Microwave Symposium Digest*, 185–187, 1979.
20. Gallium Nitride 28 V, 5 W RF Power Transistor, NPTB00004 Datasheet, 2009, http://www.nitronex.com/pdfs/NPTB00004.pdf.
21. Takayama, Y., "A new load-pull characterization method for microwave power transistors," *IEEE MTT-S International Microwave Symposium Digest*, 218–220, 1976.
22. Le, D.-L. and F. M. Ghannouchi, "Multi-tone characterization and design of FET resistive mixers based on combined active source-pull/load-pull techniques," *IEEE Transactions on Microwave Theory and Techniques*, Vol. 46, No. 9, 1201–1208, September 1998.
23. Ghannouchi, F. M., M. S. Hashmi, S. Bensmida, and M. Helaoui, "Loop enhanced passive source- and load-pull technique for high reflection factor synthesis," *IEEE Transactions on Microwave Theory and Techniques*, Vol. 58, No. 11, 2952–2959, November 2010.
24. Tektronix, "TDS794D User's Manual," http://www2.tek.com/ cmswpt/ psdetails.lotr?ct=PS&cs=psu&ci=13446&lc=EN.